Materials Research. 2016; 19(1): 1-8
DOI:http://dx.doi.org/10.1590/1980-5373-MR-2015-0504

Impedance and Modulus Spectroscopy Characterization of Tb modified $Bi_{0.8}A_{0.1}Pb_{0.1}Fe_{0.9}Ti_{0.1}O_3$ Ceramics

Shweta Thakur[a], Radheshyam Rai[a*], Igor Bdikin[b] and Manuel Almeida Valente[c]

[a]School of Physics, Shoolini University, 173229, Solan, Himachal Pradesh, India
[b]Centre for Mechanical Technology and Automation - TEMA, University of Aveiro - UA, 3810-193, Aveiro, Portugal
[c]Departamento de Fisica, I3N, Universidade de Aveiro - UA, Campus Universitario de Santiago, 3810-193 Aveiro, Portugal

Received: August 27, 2015; Accepted: November 17, 2015

In this paper we present the impedance spectroscopy of ternary solid solutions of $BiFeO_3$, $TbFeO_3$ and $PbTiO_3$, prepared by solid-state reaction method. The preliminary structural studies were carried out by x-ray diffraction technique, showing the formation of polycrystalline sample with ABO_3 type of perovskite structure with hexagonal symmetry for $Bi_{0.8}Tb_{0.1}Pb_{0.1}Fe_{0.9}Ti_{0.1}O_3$ system at room temperature. Dielectric and impedance study of this ceramic has been characterized in the temperature range 175 - 325 ^{0}C and frequency range 100 Hz - 1 MHz. The maximum ferroelectric transition temperature (T_c) of this system was in the range 210 - 225 ^{0}C with the dielectric constant having maximum value ~2480 at 1 kHz. The complex impedance graph exhibited one impedance semicircle arc at all reported temperatures, which indicates that the impedance response is a Cole-Cole type relaxation. Single semicircle indicate that the grain effect of the bulk in ceramic. The bulk resistance of the material decreases with increasing temperature showing negative temperature showing a typical semiconducting property, i.e. negative temperature coefficient of resistance (NTCR) behavior.

Keywords: *X-ray diffraction; Multiferroic; Dielectric properties; Electrical properties.*

1. Introduction

The materials exhibiting multiple ferroic properties, such as ferroelectricity, ferroelasticity, and ferromagnetism (or antiferromagnetism) in the single phase are referred to as multiferroics. The coupling between the magnetic and electronic in multiferroics, namely, magnetoelectric effect, could provide an additional degree of freedom in device design, which is more scientifically important than the ferroelectricity or magnetism individually [1,2]. Recently, ferroelectromagnetic materials have become widely known due to their potential applications in the memory devices, sensors, and spintronics [3]. There are very few materials exhibiting both ferromagnetic (FM) and ferroelectric (FE) properties at room temperature (RT), such as ($BiFeO_3$, abbreviated as BFO) and bismuth titanium iron ($Bi_3FeTi_3O_{15}$, abbreviated as BFTO) [4,5]. The ferroelectromagnetic property has been reported in several structural types of materials such as sulfide spinels and oxide perovskites [6]**.** Perovskite-type materials provide a broad range of magnetic and electrical properties covering antiferroelectric, antiferromagnetic, metallic, semiconductor, and insulator behaviours. The combination of these perovskite members could open various routes for achieving the multiferroic properties in a single phase. Recently, several groups reported on the synthesis and characterization of multiferroic perovskite systems such as $BiFeO_3$(BF) – $PrFeO_3$(PF) – $PbTiO_3$ (PT) [7] and $BiFeO_3$(BF) - $PbTiO_3$ (PT) [8] systems.

*e-mail: rshyam1273@gmail.com

$BiFeO_3$ is a perovskite system, intensively studied in recent years, due to the expectations of magnetoelectric properties at room temperature. The existence of both magnetic and ferroelectric ordering makes it a magnetoelectric material. $BiFeO_3$ has long been known to be ferroelectric with a Curie temperature of about 1103 K and antiferromagnetic with a Neel temperature (T_N) of 643 K. These high transition temperatures allow the usage of $BiFeO_3$ (BFO) for devices in a wide range of temperature. $BiFeO_3$ is one of the most extensively investigated multiferroic compound in which the Bi 6s lone pair electrons are believed to be responsible for ferroelectricity, while partially filled d orbital of Fe lead to magnetic ordering. The disadvantages of these materials are that they possess weak ferroelectric (polarization) and ferromagnetic order parameters. Large number of oxygen vacancies produced due to highly volatile nature of Bi and the multiple oxidation states of Fe (Fe^{2+} and Fe^{3+}) cause a high leakage current in the material that degrades its ferroelectric properties [9-11]. In order to (i) enhance ferroelectric (polarization) and ferromagnetic order parameters and (ii) reduce leakage current several attempts have been made to replace A and B site of pure $BiFeO_3$ using proper dopants like Ba^{2+}, Sr^{2+}, Ca^{2+}, La^{3+}, Gd^{3+}, Ti^{4+}, Mn^{4+}, Nb^{5+} etc. Preparation of pure $BiFeO_3$ in the bulk ceramic form without traces of impurities has been a very difficult task[12]. Sosnowska et al., have prepared $BiFeO_3$ in the bulk but ended up with a few traces of $Bi_2Fe_4O_9$ [13]. At present, there are two ways used to solve the problems, one is doping at B-Site with other perovskite (e.g., ferroelectric $PbTiO_3$, $BaTiO_3$ and $SrTiO_3$) [14] with $BiFeO_3$

in order to stabilize a perovskite structure formation and to enhance the electric insulation resistance. Another way is to add other dopants, e.g., gallium [15], tantalum, neodymium [16], or other rare-earth materials to improve the magnetic properties [17] . Therefore, $BiFeO_3$-ABO_3 solid solution systems have attracted great attention as a means to increase structural stability and sintering ability.

Yao et al., have prepared a bulk ternary (0.85-x) ($BiFeO_3$)-$x$$BaTiO_3-0.15PbTiO_3$ (BF-xBT-PT, x=0.08-0.35) system which shows piezoelectric constant d_{33} of 60 pC/N, high Curie temperature of 550 ^{0}C, and low sintering temperature of 920 ^{0}C [18]. Mazumder. synthesised Pb-doped $BiFeO_3$ powders were found that bulk densities increased up to 93% of theoretical density and dielectric properties also improved by the Pb-doping as compare to pure $BiFeO_3$ [19] . The orthoferrites with the formula $RFeO_3$ (R is a rare-earth element and M is a transition metal atom) have been reported by a number of authors [20,21]. These orthoferrites are the G-type antiferromagnets with weak ferromagnetism and good electrical insulators. It is known that the perovskite structure has the ability to stabilize cations in unusually high oxidation states, and the anion sublattice can accommodate a high concentration of vacant sites. Lotey et al., have synthesised Tb-doped $BiFeO_3$ nanowires and reported that increases in Tb concentration, the saturation magnetization increases and leakage current density decreases [22]. Zhang et al., have prepared a series of rare-earth doped $BiFeO_3$ ($Bi_{1-x}R_xFeO_3$ (x=0–1, R = La, Nd, Sm, Eu and Tb), samples and reported structure transformation from rhombohedral lattice to orthorhombic by increasing x. Neel temperature and magnetisation also enhanced by the doping of rare earth ions [18] . Kumar et al., synthesised the Tb-Mn co-substituted $BiFeO_3$ ($Bi_{1-x}Tb_xFe_{1-x}Mn_xO_3$, x = 0, 0.10, 0.15, 0.20) by a solid-state reaction method and have reported a very high transition temperature ~ 820 ^{0}C [23] . In this study, the crystal structure, dielectric and electric properties of the ternary perovskite system $Bi_{0.8}Tb_{0.1}Pb_{0.1}Fe_{0.9}Ti_{0.1}O_3$, a combination of three ternary pervoskite systems, 2 Ferromagnetic and 1 Ferroelectric have been prepared. Tb were used to substitute at the A site of sample, because their radii are similar to each other (Atomic radii of Tb = 225 pm), and they stabilize the perovskite phase that helps to decrease the Bi volatilization and the amount of oxygen vacancies.

2. Experimental

Polycrystalline samples of $Bi_{0.8}Tb_{0.1}Pb_{0.1}Fe_{0.9}Ti_{0.1}O_3$ were synthesized from high purity oxides Bi_2O_3 (99.9% pure M/S Aldrich chemicals USA), Fe_2O_3 (99.9% pure M/S Aldrich chemicals, USA), Tb_4O_7 (99.9% pure M/S Aldrich chemicals, USA), PbO (99.9% pure M/S Aldrich chemicals, USA) and TiO_2, (99.9% pure M/S Aldrich chemicals, USA), using high temperature solid-state reaction technique. The constituent compounds in suitable stoichiometric were thoroughly mixed in a ball milling unit for 48 h. Then powder was dried at 125 °C and calcined at 800 °C for 4 h in alumina crucibles. The calcined fine powder was cold pressed into cylindrical pellets of 10 mm in diameter and 1-2 mm in thickness using a hydraulic press with a pressure of 50 MPa. These pellets were sintered at 850°C for 4 h. The formation and quality of compounds were verified with X-ray diffraction (XRD) technique. The XRD patterns of the compounds were recorded at room temperature using X-ray powder diffractometer (Rigaku Minifiex, Japan) with CuKα radiation (λ = 1.5405 Å) in a wide range of Bragg angles 2θ (20° ≤ 2θ ≤ 60°) at a scanning rate of 1/2° min^{-1}. The dielectric constant (ε) and loss tangent (tanδ) of the compounds were measured using a HP 4284A Precision LCR meter as a function of frequency at room temperature (RT) and temperature (RT to 300 °C) at different frequencies with a home-made furnace.

3. Results and discussion

Fig. 1 shows the XRD patterns of $Bi_{0.8}Tb_{0.1}Pb_{0.1}Fe_{0.9}Ti_{0.1}O_3$ ceramics at room temperature. All patterns showed that the samples have a pure phase with a Hexagonal structure at room temperature (JCPDS card no.- 742497 $Bi_{0.8}Pb_{0.2}Fe_{0.8}Ti_{0.2}O_3$). All the reflection peaks were indexed using observed inter-planar spacing d, and lattice parameters of $Bi_{0.8}A_{0.1}Pb_{0.1}Fe_{0.9}Ti_{0.1}O_3$ were determined by using least-squares refinement method. The calculated and observed d values of all diffraction lines (reflections) of the above compounds are shown in Table 1. Because of the kinetics of the formation, mixtures of $BiFeO_3$ are always obtained as a major phase along with other impurity phases during synthesis. The little impurity phase was observed which it is shown as * in Fig. 1. It may be attributed to $Bi_2Fe_4O_9$. As for $BiFeO_3$, it is difficult task to prepare a pure $BiFeO_3$ compound and the available literature indicates that a small impurity concentration is always present in the system [13].

All the reflection line in XRD pattern were used for obtaining the average crystalline size using the Debye-Scherrer equation, [24]

$$t = \frac{0.9\lambda}{B\cos\theta_B} \quad (1)$$

$$B = \left(B_M^2 - B_S^2\right)^{1/2} \quad (2)$$

where t is the diameter of the particle, λ is the x-ray wavelength (0.154 nm), B_M and B_S are the measured peak broadening and instrumental broadening in radian, respectively, and θ_B is the Bragg angle of the reflection.

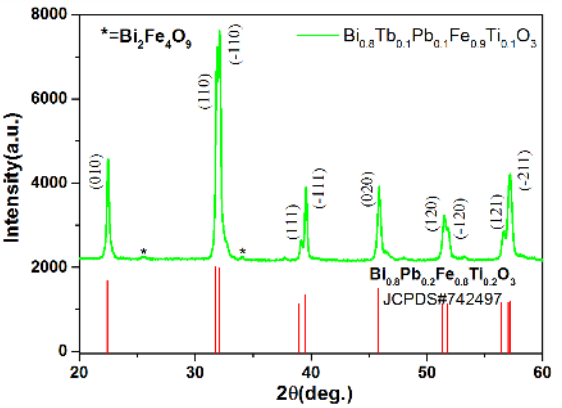

Fig. 1 Room temperature XRD patterns of $Bi_{0.8}Tb_{0.1}Pb_{0.1}Fe_{0.9}Ti_{0.1}O_3$ ceramics.

The calculated average crystalline size from Eq. (1) is 30-40nm.

Fig. 2(a-b) shows the variation of dielectric constant (ε) and loss tangent (tan δ) as a function of applied frequency of $Bi_{0.8}Tb_{0.1}Pb_{0.1}Fe_{0.9}Ti_{0.1}O_3$ ceramic at different temperatures. As shown in the Fig. 2(a) dielectric constant (ε) and loss tangent (tan δ) decreases with increasing frequency from 100Hz to 1MHz [25]. Initially dielectric constant (ε) and loss tangent (tan δ) decreases sharply and after that it decreases smoothly. As $Bi_{0.8}Tb_{0.1}Pb_{0.1}Fe_{0.9}Ti_{0.1}O_3$ ceramic have maximum value of dielectric constant ~13580 at 350 ^{0}C. On the other hand, the maximum value of loss tangent factors (tan δ) is ~79 at 350 ^{0}C. The dielectric constant of any material is due to the dipolar, electronic, ionic, and interfacial polarizations. At low frequencies, dipolar and interfacial polarizations are responsible for the dielectric behavior of the material. However, at higher frequencies electronic polarization is responsible for the dielectric and contribution of dipolar polarization becomes insignificant. The decrease in dielectric constant with increased frequency could be explained on the basis of dipole relaxation phenomenon [26].

Fig. 3(a-b) shows the variation of dielectric constant (ε) and loss tangent (tanδ) with temperature at different frequencies 1 kHz, 10 kHz and 100 kHz, which was obtained on silver electrode samples in plane capacitor configuration. The two peaks were observed, the first peak corresponds to the ferroelectric-ferroelectric (FE-FE) and second peak correspond to the ferroelectric–paraelectric (FE-PE) phase transition [27,28]. These peaks are due to two different ferroelectric compounds present in the ceramic system i.e. $BiFeO_3$ and $PbTiO_3$. As in normal ferroelectrics, the dielectric constant of $Bi_{0.8}Tb_{0.1}Pb_{0.1}Fe_{0.9}Ti_{0.1}O_3$ increases upto transition temperature then decreases with increasing temperature. In Fig. 3(b) the dielectric loss increases smoothly up to 275 ^{0}C but after this temperature the loss increases sharply. $Bi_{0.8}Tb_{0.1}Pb_{0.1}Fe_{0.9}Ti_{0.1}O_3$ ceramic have maximum value of dielectric constant ~2500 and the maximum value of loss tangent (tan δ) is ~600 at 1 kHZ. This high conductivity and leakage, especially at higher temperatures in $BiFeO_3$-based ceramics were considered to be caused in part by the difficulty of producing this material in its single phase. Therefore, the problem persists even in very pure $BiFeO_3$ ceramics and it was explained as originating from the spontaneous change of the oxidation state of Fe^{3+}/Fe^{2+} [29,30] . This change is responsible for the formation of oxygen vacancies for preserving the local electrical neutrality and causes thermally activated hopping conduction. In addition, an important contribution to the losses may occur in bulk ceramics by defects associated

Table 1. Lattice parameters of $Bi_{0.8}Tb_{0.1}Pb_{0.1}Fe_{0.9}Ti_{0.1}O_3$ ceramics.

Composition	Crystal System	Lattice Parameter	d_{obs}	d_{cal}	hkl
BTPFT	Hexagonal	a = 5.5728Å c = 6.9257Å α, β = 90˚ γ = 120˚	3.9586	3.9596	(010)
			2.8133	2.8135	(110)
			2.7868	2.7864	(-110)
			2.3081	2.3085	(111)
			2.2789	2.2787	(-111)
			1.9799	1.9798	(020)
			1.7775	1.7777	(120)
			1.7640	1.7640	(-120)
			1.6295	1.6297	(121)
			1.6137	1.6139	(-121)
			1.6088	1.6087	(-211)

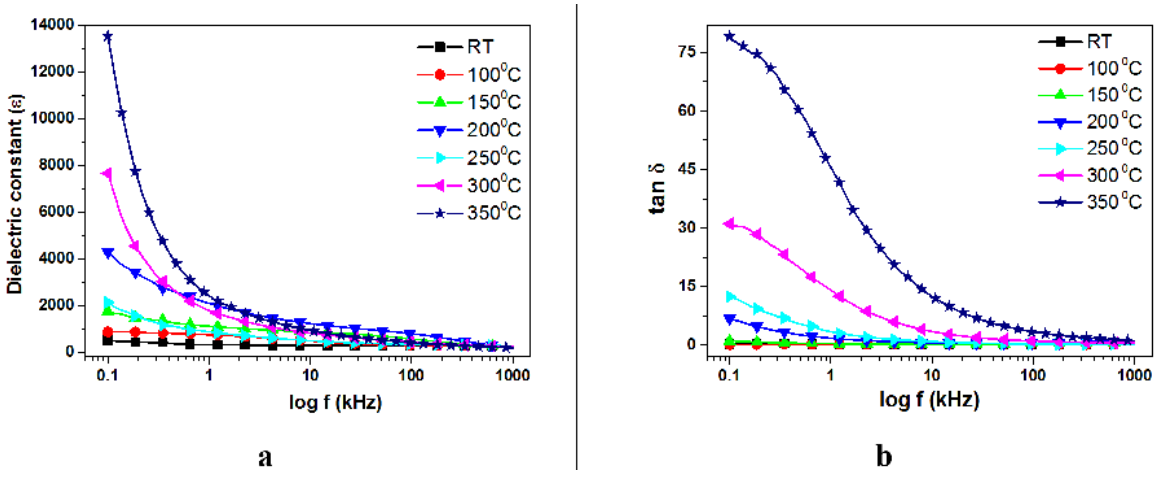

Fig. 2(a-b) Variation of dielectric constant (ε) and loss tangent (tan δ) of $Bi_{0.8}Tb_{0.1}Pb_{0.1}Fe_{0.9}Ti_{0.1}O_3$ ceramics with frequency at different temperatures.

with the grain boundaries. All these phenomena often make difficult the detection of the ferroelectric-paraelectric phase transition by polarization hysteresis measurements. This phase transition has diffuse character which can be understood in terms of the inhomogeneous distribution of ions in A and B sites of the ABO_3 perovskite cell. Above the transition temperature it does not follow the Curie-Weiss law as predicted by thermodynamic theory. Value of dielectric constant and loss tangent at room temperature and transition temperature (Curie temperature, T_c) and dielectric constants are mentioned in Table 2 at different frequencies 1 kHz, 10 kHz and 100 kHz.

The electrical properties of $Bi_{0.8}Tb_{0.1}Pb_{0.1}Fe_{0.9}Ti_{0.1}O_3$ material were investigated by a complex impedance spectroscopy (CIS) technique. It is important to transform the dielectric and electrical data in different formalism and analyze them to get real picture of the material. The use of function Z* is particularly appropriate for the resistive and/or conductive analysis where the long-range conduction dominates, where as the ε* and M* functions are suitable when localized relaxation dominates. So the plotting of ac data in terms of impedance, electric modulus, and dielectric permittivity simultaneously gives a complete assignment of all the physical processes taking place in the material.

Fig. 4 shows the temperature-dependent spectra (Nyquist plot) of $Bi_{0.8}Tb_{0.1}Pb_{0.1}Fe_{0.9}Ti_{0.1}O_3$ material. By impedance spectrum we got the single semicircular arc in temperature range 175 – 325 ^{0}C. The nature of variation of the arcs with temperature and frequency provides various clues of the materials. This single semicircular arc suggests the presence of grain interior (bulk) property of the material. The high frequency semicircle arc can be attributed to the bulk (grain) properties of the material. The impedance spectra are characterized by the appearance of a single semicircular arc and the intercept of the semicircular arc with the real axis (Z′) gives us an estimate of the bulk resistance (R_b) of the material. It has been observed that the bulk resistance of the material decreases with increase in temperature showing a typical semiconducting property, i.e. negative temperature coefficient of resistance (NTCR) behavior. Fig. 5 shows the fitting from 175 ^{0}C to 325 ^{0}C of Nyquist plot respectively. It is observed that with the increase in temperature the slope of the lines are decreases and the lines bend towards real (Z′) axis. A semicircle of the graph indicating that conductivity of the sample increases. It can also be observed that the peak maxima of the plots decrease and the frequency for the maximum shifts to higher values with the increase in temperature. It can be noticed that the complex impedance plots are not represented by full semicircle, rather the semicircular arcs are depressed and the centre of the arcs lies below the real (Z′) axis suggesting the relaxation to be of poly dispersive non-Debye type in samples. This may be due to the presence of distributed elements in the material electrode system [31]. An equivalent circuit is being used to provide a complete picture of the system and establish the structural property relationship of the materials. Comparison of complex impedance plots (symbols) with fitted data (lines) using commercially available software ZSimpwin Version 2 has been given in the fig. To model the non-Debye response, constant phase element (CPE) is used in addition to resistors and capacitors.

Fig. 6(a) shows the variation of real part of impedance (Z′) as a function of frequency at different temperatures. The pattern shows a sigmoid variation as a function of frequency

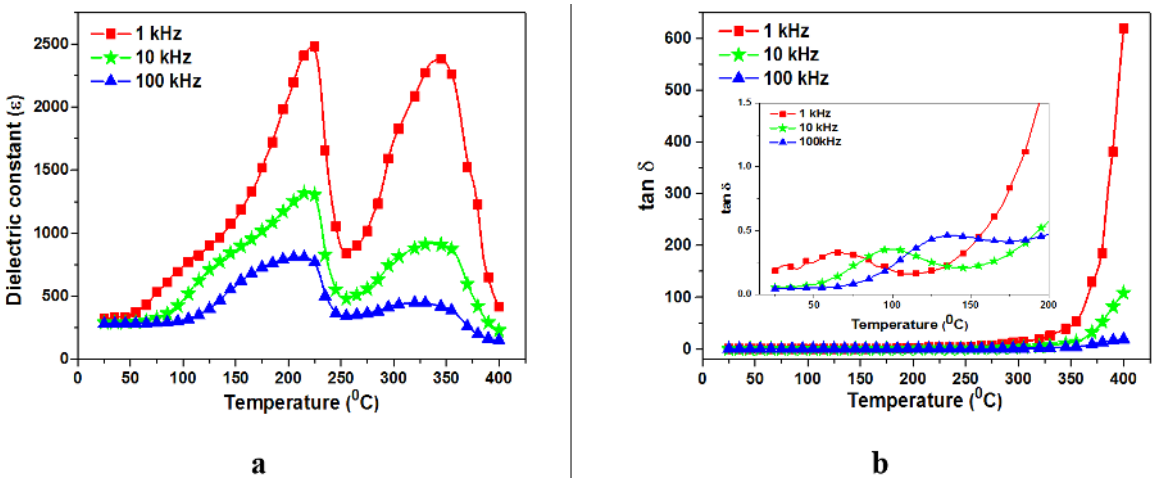

Fig. 3(a-b) Variation of dielectric constant (ε) and loss tangent (tan δ) of $Bi_{0.8}Tb_{0.1}Pb_{0.1}Fe_{0.9}Ti_{0.1}O_3$ ceramics with temperatures at frequency 1 kHz, 10 kHz and 100 kHz.

Table 2. Details of the physical parameters of $Bi_{0.8}Tb_{0.1}Pb_{0.1}Fe_{0.9}Ti_{0.1}O_3$ ceramics.

Sample Name	Frequency (KHz)	$T_{max(FE-FE)}$ (^{0}C)	$\varepsilon_{max(FE-FE)}$	$T_{max(FE-PE)}$ (^{0}C)	$\varepsilon_{max(FE-PE)}$
BTPFT	1	225	2480	345	2385
	10	220	1380	335	920
	100	210	811	325	451

in the low frequency region followed by a saturation region in the high frequency region. This suggests the presence of mixed nature of polarization behavior in the material, such as electronic, dipolar and orientation polarization. A decreasing trend of Z′ with rise in temperature suggests the presence of negative temperature coefficient of resistance (NTCR) in the material in the low frequency region but tends to merge in the high frequency region at almost all temperatures. These results indicate a possibility of increase in ac conductivity with rise in temperature in the high frequency region which is due to the release of space charge and lowering in the barrier properties of the material. Fig. 6(b) presents the variation of imaginary part of impedance (Z″) as a function of frequency at different set of temperatures. With the increase of frequency, imaginary part of impedance (Z″) decreases with increase of frequency. The magnitude of Z″ decreases with increasing temperature. This would imply that dielectric relaxation is temperature dependent, and there is apparently not a single relaxation time which are sported by the results reported by Pattanayak S. in Gd-doped $BiFeO_3$ sample [32].

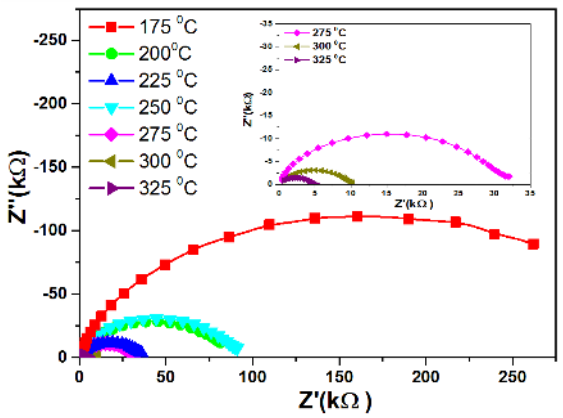

Fig. 4 Nyquist plot of $Bi_{0.8}Tb_{0.1}Pb_{0.1}Fe_{0.9}Ti_{0.1}O_3$ ceramics at different temperatures.

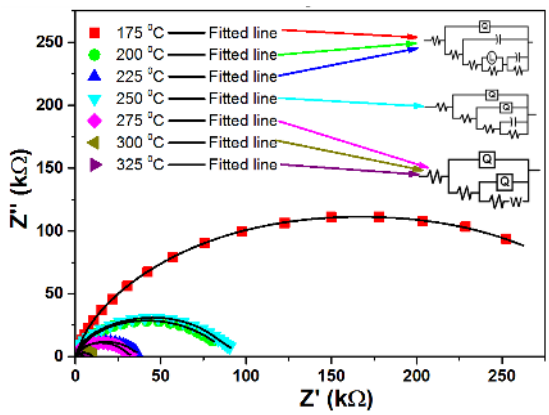

Fig. 5 Fitting of Cole-Cole plot of $Bi_{0.8}Tb_{0.1}Pb_{0.1}Fe_{0.9}Ti_{0.1}O_3$ ceramics.

Complex modulus analysis is an alternative approach to explore electrical properties of the material and to magnify any other effects present in the sample. It is an important and convenient tool to determine, analyse and interpret the dynamical aspects of electrical transport phenomena (i.e. parameters such as carrier/ion hopping rate, conductivity relaxation time, etc.). In order to analyse and interpret the experimental data, it is essential to have a model equivalent circuit that provides a realistic representation of the electrical properties. The complex electric modulus spectrum M′ versus M″ is shown in Fig. 7 for $Bi_{0.8}Tb_{0.1}Pb_{0.1}Fe_{0.9}Ti_{0.1}O_3$ ceramics at different temperatures. The patterns are characterized by the presence of little asymmetric and depressed semicircular arcs whose centre does not lie on M′ axis. The behaviour of electric modulus spectrum is suggestive of the temperature dependent hopping type of mechanism for electric conduction (charge transport) in the system and non-Debye type dielectric relaxation.

Fig. 8(a) shows the variation of Real part (M′) of modulus with frequency at different temperatures of $Bi_{0.8}Tb_{0.1}Pb_{0.1}Fe_{0.9}Ti_{0.1}O_3$ ceramics. The variation of M′ with frequency shows a dispersion tending towards M_∞ (the asymptotic value of M′ at higher frequencies) and it (dispersion) shifts towards higher frequency side as temperature increases. The asymmetric plot of M′ is because of the stretched exponential character of relaxation time of the material. Monotonous dispersion on increasing frequency

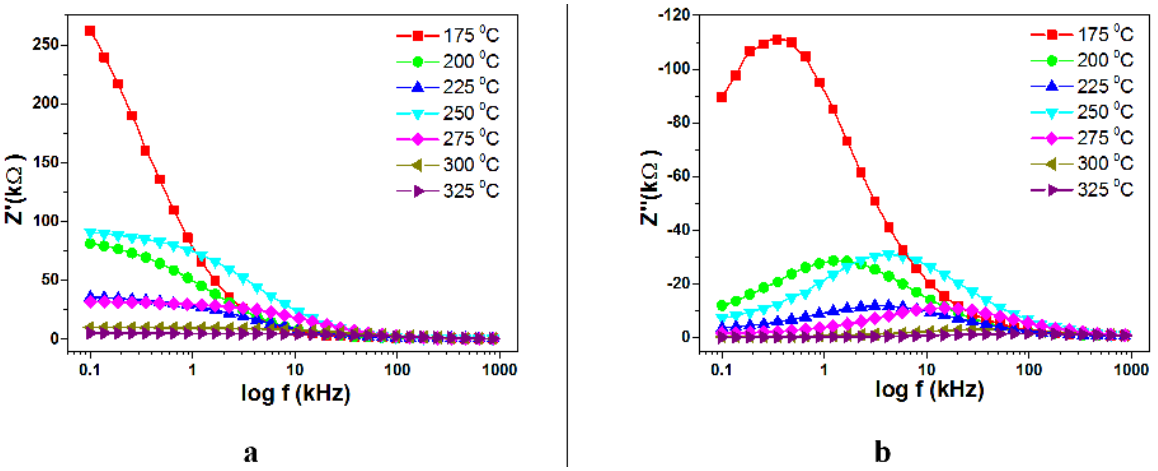

Fig. 6(a-b) Variation of real part (Z′) and imaginary part (Z″) of impedance with frequency at different temperatures of $Bi_{0.8}Tb_{0.1}Pb_{0.1}Fe_{0.9}Ti_{0.1}O_3$ ceramics.

at lower temperatures may be caused by short range mobility of charge carriers. Such results may possibly be related to a lack of restoring force governing the mobility of the charge carriers under the action of an induced electric field. Fig. 8(b) shows the variation of imaginary part of modulus (M″) with frequency at different temperatures. From this graph we found that M″ shows the strong peaks and the position of the peak i.e. M''_{max} shifted to higher frequencies as the temperature was increased. The frequency region below peak maximum M″ determines the range in which charge carriers are mobile on long distances. At frequency above peak maximum, the carriers are confined to potential wells, being mobile on short distances. The peaks are asymmetric and broader than the ideal Debye curve. The frequency range where the peaks occur is indicative of transition from long range to short range mobility.

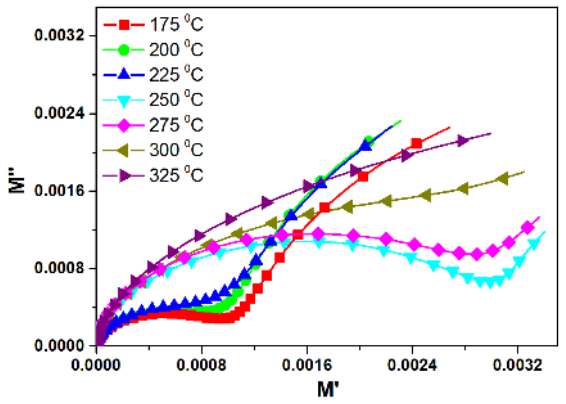

Fig. 7 Variation of real and imaginary part of modulus at different temperatures of $Bi_{0.8}Tb_{0.1}Pb_{0.1}Fe_{0.9}Ti_{0.1}O_3$ ceramics.

Fig. 9(a-b) shows the normalized plot of Z''/Z''_{max} and M''/M''_{max} versus log (f/f_{max}) at different temperatures for $Bi_{0.8}Tb_{0.1}Pb_{0.1}Fe_{0.9}Ti_{0.1}O_3$ ceramics respectively. The normalized plot overlaps on a single master curve at different temperatures (i.e. same shape and pattern in the peak position with slight variation in full width at half maximum FWHM with rise in temperature). Thus the dielectric processes occurring in the material can be investigated via master modulus plot. The value of FWHM evaluated from the normalized spectrum is greater than log $\frac{2+\sqrt{3}}{2-\sqrt{3}}$, and this indicates about

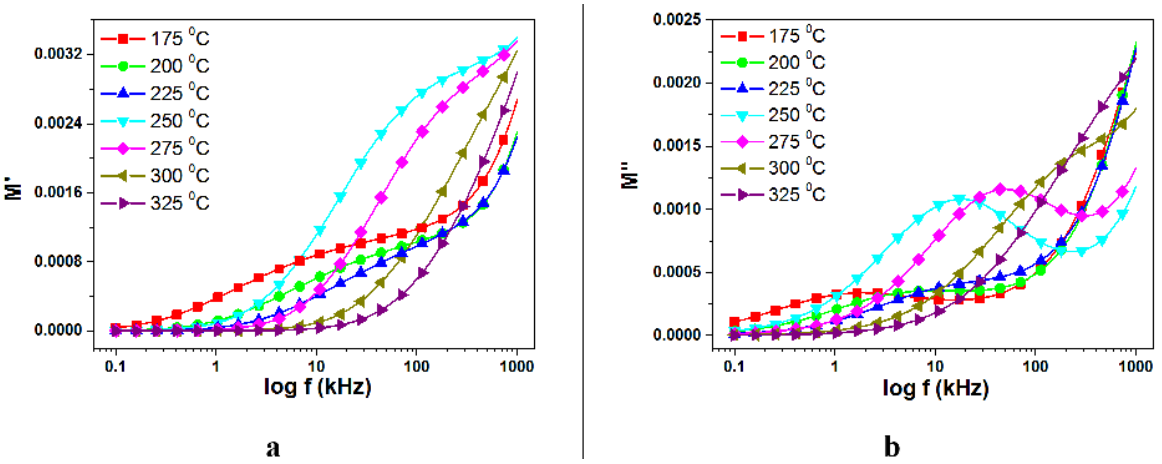

Fig. 8 (a-b) Variation of real part (M″) and imaginary part (M″) of modulus with frequency at different temperatures of $Bi_{0.8}Tb_{0.1}Pb_{0.1}Fe_{0.9}Ti_{0.1}O_3$ ceramics.

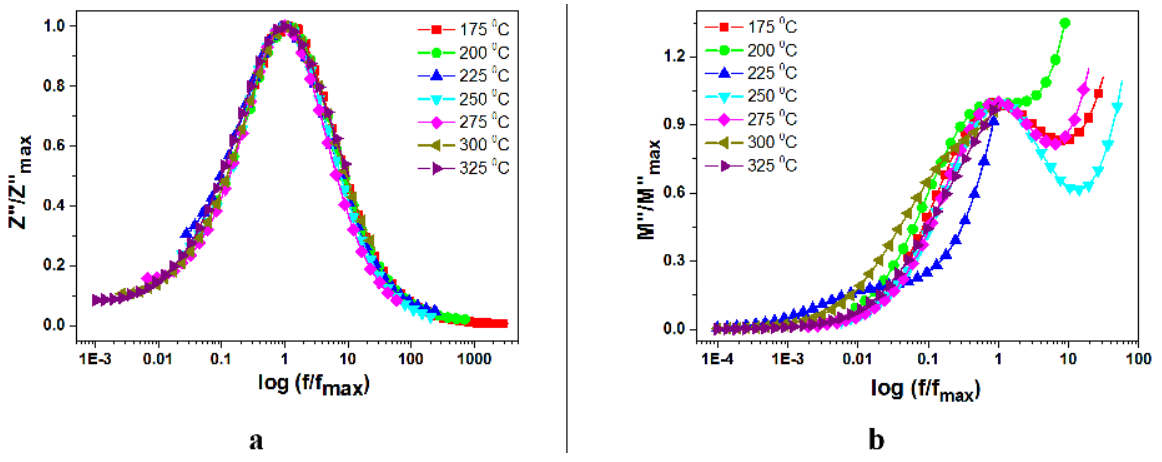

Fig. 9(a-b) Modulus scaling behavior of compounds in the master curves of $Bi_{0.8}Tb_{0.1}Pb_{0.1}Fe_{0.9}Ti_{0.1}O_3$ ceramics.

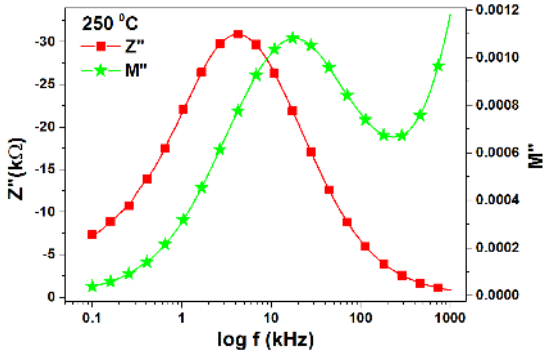

Fig. 10 Variation of Z″ and M″ with frequency at (250 ^{0}C) temperature of $Bi_{0.8}Tb_{0.1}Pb_{0.1}Fe_{0.9}Ti_{0.1}O_3$ ceramics.

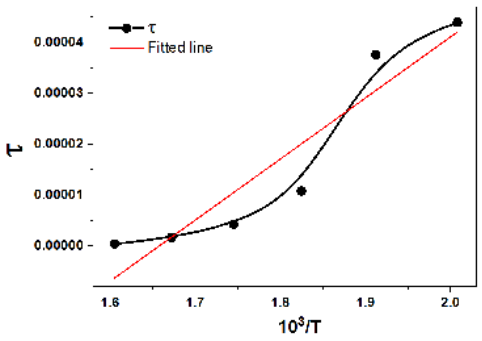

Fig. 11. Variation of relaxation time (calculated from impedance) with temperature.

non-Debye type behavior which is well supported by complex modulus plot [33].

Fig. 10 shows the comparison of the frequency-dependent behavior of M″ and Z″ for the sample at temperature 250 ˚C. It was found that there is a wide gap between M″ and Z″ peaks showing the Non Debye type of behaviours. The Z″ peaks are asymmetric at lower frequency side while M″ peak are asymmetric on the higher frequency side. In the entire range of observed temperature no overlapping temperature could be found, indicating that the samples have component both from long range conductivity and localized relaxation.

Fig. 11 shows the nature of variation of relaxation time with temperature of the compounds for impedance plot. The frequency ω (corresponding to Z''_{max}) gives the most probable relaxation time τ. All the curves find to follow the Arrhenius relation:

$$= \tau_0 \exp\left(\frac{E_a}{kT}\right)$$

Where τ_0 is pre-exponential factor, Ea is the activation energy, k is Boltzmann constant and T is the absolute temperature. The τ value of the $Bi_{0.8}Tb_{0.1}Pb_{0.1}Fe_{0.9}Ti_{0.1}O_3$ ceramics was found to be decreasing with increasing temperature, which is a typical behavior of a semiconductor. The semiconducting nature of the grains in ceramics is believed to be due to the loss of oxygen during high temperature sintering process. The values of Ea show that the dielectric relaxation processes in the samples are closely related to the oxygen vacancies, which have been reported as the most mobile ionic defects in perovskite [34] . The activation energy in the ABO_3 perovskite structure decreases with increasing oxygen vacancy content [35].

4. Conclusions

Ternary solid solutions of $BiFeO_3$, $TbFeO_3$ and $PbTiO_3$ have been prepared by solid-state reaction method. The XRD pattern confirms that sample has a hexagonal structure at room temperature. Dielectric properties of sample have been studied in the temperature range between 175 - 325 ^{0}C and frequency range 100 Hz - 1 MHz. The maximum ferroelectric transition temperature (T_c) of this system was in the range 210 - 225 ^{0}C with the dielectric constant of ~2480 at 1 kHz. Impedance spectroscopy there is the presence of single semicircle arc at all reported temperatures which indicates that there is presence of grain interior (bulk) property in material. Sample showed dielectric relaxation, which is found to be of non-Debye type and the relaxation frequency shifted to higher side with the increase of temperature. The Nyquist plot and conductivity studies showed the negative temperature coefficient of resistance behavior (NTCR) of samples. These materials have used tremendous applications in the form of sensor, actuator and transducer.

References

1. Fiebig M, Lottermoser T, Fröhlich D, Goltsev AV, Pisarev RV. Observation of coupled magnetic and electric domains. *Nature*. 2002;419(6909):818-20.
2. Efremov DV, van den Brink J, Khomskii DI. Bond- versus site-centred ordering and possible ferroelectricity in manganites. *Nature Materials*. 2004;3(12):853-6.
3. Park TJ, Papaefthymiou GC, Viescas AJ, Moodenbaugh AR, Wong SS. Size-dependent magnetic properties of single-crystalline multiferroic BiFeO3 nanoparticles. *Nano Letters*. 2007;7(3):766-72.
4. Park BH, Hyun SJ, Bu SD, Noh TW, Lee J, Kim HD, Kim TH, Jo W. Differences in nature of defects between $SrBi_2$ Ta_2 O_9 and Bi_4 Ti_3 O_{12}. *Applied Physics Letters*. 1999;74:1907.
5. Karl TR, Trenberth KE. Modern global climate change. *Science*. 2003;302(5651):1719-23.
6. Hemberger J, Lunkenheimer P, Fichtl R, Krug von Nidda HA, Tsurkan V, Loidl A. Relaxor ferroelectricity and colossal magnetocapacitive coupling in ferromagnetic CdCr2S4. *Nature*. 2005;434(7031):364-7.
7. Saito Y, Takao H, Tani T, Nonoyama T, Takatori K, Homma T, Nagaya T, Nakamura M. Lead-free piezoceramics. *Nature*. 2004;432(7013):84-87.
8. Mishra K, Satya A, Bharathi A, Sivasubramanian V, Murthy V, Arora A. Vibrational, magnetic, and dielectric behaviro of La-substituted BiFe [o.sub.3]-PbTi 3, [bismuth iron]. *Journal of Applied Physics*. 2011;110:123529.
9. Cheng Z, Wang X, Dou S, Kimura H, Ozawa K. Improved ferroelectric properties in multiferroic Bi Fe O3 thin films

through La and Nb codoping. *Physical Review B.* 2008;77: 092101.

10. Makhdoom AR, Akhtar MJ, Rafiq MA, Hassan MM. Investigation of transport beheavior in Ba dopode BiFe03. *Ceramics International.* 2012;38(5):3829-3834.
11. Shami M, Awan M, Anis-ur-Rehman M. Effect of sintering temperature on nanostructured multiferroic BiFe)3 ceramics. *Key Engineering Materials.* 2012;510:348-355.
12. Rai R, Bdikin I, Valente MA, Kholkin AL. Ferrolectric and ferromagnetic properties of Gd-doped BiFe)-3BaTi)3 solid solution. *Materials Chemistry and Physics,* 119 (2010) 539-545.
13. Sosnowska I, Neumaier TP, Steichele E. Spiral magnetic ordering in bismuth ferrite. *Journal of Physics C: Solid State Physics.* 1982;15:4835-4836.
14. Kumar MM, Srinivas A, Suryanarayana SV. Structure property relations in BiFO3/BaTiO3 solid solutions. *Journal of Applied Physics.* 2000;87:855-862.
15. Cheng JR, Li N. Cross, structural and dielectric properties of Ga-modified $BiFe)_3$-$PbtiO_3$ crystalline solution. LE. *Journal of Applied Physics.* 2003*;94* 5153-5157.
16. Mathe V, Patankar K, Patil R, Lokhande C. Synthesis and dielectric properties of $Bi_{1-x}Nd_xFeO_3$ perovskites. *Journal of Magnetism and Magnetic Materials.* 2004*;270*:380-388.
17. Rai R, Bdikin I, Valente MA, Kholkin AL. Ferroelectric and magnetic properties of perovskite structured Bi1-x-yGdxBayFe1yTiyO3 magnetoelectric ceramic. *Journal of Advanced Dielectrics* 2011;1:257-267. DOI: 10.1142/S2010135X11000318
18. Yao Z, Liu Y, Song Z, Wang Z, Hao H, Cao M, Yu Z, Liu H. Structure and electrical properties of ternary BiFeO 3 -BaTiO 3 -PbTiO 3 high-temperature piezoceramics. *Journal of Advanced Ceramics*. 2012;1:227-231.
19. Mazumder R, Sen A. Effect of Pb-doping on dielectric properties of BiFeO 3 ceramics. *Journal of Alloys and Compounds*. 2009;475:577-580.
20. Jaeger R, Egerton L. Hot pressing of potassium-sodium niobates. *Journal of the American Ceramic Society*. 1962;45:209-213. DOI: 10.1111/j.1151-2916.1967.tb15121.x
21. Haertling G. Properties of Hot-pressed ferroelectric alkali niobate ceramics. *Journal of the American Ceramic Society.* 1967;50:329-330.
22. Lotey GS, Verma N. Multiferroic propertiers of Tb-doped $BiFeO_3$ nanowires. *Journal of Nanoparticle Research.* 2013*;15*:1553.
23. Saravana K, Ashwini P, Venkateswaran C. Effect of Tb–Mn substitution on the magnetic and electrical properties of BiFeO 3 .*Journal of Magnetism and Magnetic Materials*. 2014; 364:60-67.
24. Patterson AL. The Scherrer formula for X-ray particle size determination. *Physical Review*. 1939;56 :978-982.
25. Rukmini HR, Choudhary RN, Rao VV. Effect of doping pairs (La, Na) on structural and electrical properties of PZT ceramics. *Materials Chemistry and Physics*. 1998;55(2):108-114.
26. Varshney D, Kumar A, Verma K. Effect of A site and B site doping on structural, thermal, and dielectric properties of BiFeO 3 ceramics. *Journal of Alloys and Compounds*. 2011;509(33):8421-8426.
27. Patterson EA, Cann DP, Pokorny J, Reaney IM. Electromechanical strain in $Bi(Zn_{1/2}Ti_{1/2})O_3$–$(Bi_{1/2}Na_{1/2})TiO_3$–$(Bi_{1/2}K_{1/2})TiO_3$ solid solutions. *Journal of Applied Physics.* 2012;111. http://dx.doi.org/10.1063/1.4714346
28. Lin D, Zheng Q, Li Y, Wan Y, Li Q, Zhou W. Microstructure, ferroelectric and piezoelectric properties of Bi0.5K0.5TiO3-modified BiFeO3–BaTiO3 lead-free ceramics with high Curie temperature. *Journal of the European Ceramic Society.* 2013:33(15-16):3023-3036.
29. Kholkin AL, Bdikin IK, Shvartsman VV, Pertsev NA. Anomalous polarization inversion in ferroelectrics via scanning force microscopy. *Nanotechnology.* 2007;18(9):095502.
30. Rai R, Valente MA, Bdikin I, Kholkin AL, Sharma S. Enhanced ferroelectric and magnetic properties of perovskite structured Bi1−*x*−*y*Gd*x*La*y*Fe1−*y*Ti*y*O3 magnetoelectric ceramics. *Journal of Physics and Chemistry of Solids*. 2013;74(7) :905-912.
31. Zha S, Xia C, Meng G. Effect of Gd (Sm) doping on properties of ceria electrolyte for solid oxide fuel cells. *Journal of Power Sources*. 2003;115(1):44-48.
32. Pattanayak S, Parida B, Das PR, Choudhary R. Impedance spectroscopy of Gd-doped $BiFeO_3$ multiferroics. *Applied Physics A.* 2013;112:387-395.
33. Shukla A, Choudhary R, Thakur A. Effect of Mn4+ substitution on thermal, structural, dielectric and impedance properties of lead titanate. *Journal of Materials Science: Materials in Electronics.* 2009;20:745-755.
34. Eichel RA. Defect structure of oxide ferroelectrics—valence state, site of incorporation, mechanisms of charge compensation and internal bias fields. *Journal of Electroceramic.* 2007;19:11-23.
35. Scott J, Dawber M. Oxygen-vacancy ordering as a fatigue mechanism in perovskite ferroelectrics. *Applied Physics Letters*. 2000;76:3801-3803.